

Numerical investigation of the interaction between the martensitic transformation front and the plastic strain in austenite

Julia Kundin ^{a,*}, Evgeny Pogorelov ^a Heike Emmerich ^a

^a*Material and Process Simulation (MPS), University of Bayreuth, DE-95448
Bayreuth, Germany*

Abstract

Phase-field simulations of the martensitic transformation (MT) in the austenitic matrix, which has already undergone the plastic deformation, are carried out. For this purpose the elasto-plastic phase-field approach of incoherent MT developed in the previous work [Kundin et. al. J. Mech. and Phys. Solids 59 (2011) 2012] is used. The evolution equation for the dislocation density field is extended by taking into account the thermal and athermal annihilation of the dislocations in the austenitic matrix and the athermal annihilation at the transformation front. It is shown that the plastic deformation in the austenite caused by the MT interacts with the pre-deformed plastic strain that leads to the inhomogeneous increasing of the total dislocation density. During the phase transformation one part of the dislocations in the pre-deformed austenite is inherited by the martensitic phase and this inheritance depends on the crystallography of MT. An other part of dislocations annihilates at the transformation front and decreases the dislocation density in the growing martensite. Based on the simulation results a phenomenological dependency of the inherited dislocations on the martensitic fraction and the plastic deformation in the martensite and austenitic matrix is proposed.

Key words: Martensitic transformation, Elasto-plastic phase-field modeling, Plastic accommodation

* Corresponding author.

Email address: Julia.Kundin@uni-bayreuth.de (Julia Kundin).

1 Introduction

The morphology of the martensitic microstructures is strongly related to the mechanical properties of steel and alloys. It is important to predict the formation of martensitic microstructure precisely. Furthermore, during the MT the incremental elastic strain energy is reduced by the formation of a heterogeneous array of different orientation variants of the martensitic phase and by plastic deformation (plastic accommodation). The development of appropriate models allows to calculate the strains associated with the phase transformation. The understanding and control of localized plasticity and its interaction with the transformation front is quite essential e.g. for TRIP-steels and shape memory alloys [1,2,3].

Recently, phase-field (PF) models have been extensively studied as a powerful tool for predicting microstructural evolution and applied to the martensitic transformation. Khachaturyan and co-workers developed the phase-field microelasticity (PFM) theory [4,5,6], which integrates microelasticity into the phase-field model employing the fast Fourier transform algorithm. The model has further applied to investigate the MT in single crystals [7] and polycrystalline systems [8] as well as for the MT with external stresses. It has been successfully applied to various coherent phase transformations including the prediction of many complicated strain-induced morphological patterns [9,10,11,12,13].

Besides the coherent phase transformations the MT in technical alloys is usually associated with plastic strains. The effect of plasticity, which can be represented as the generation and the motion of dislocations on the MT, is very complex. On the one hand, if the MT is caused by applied loads, the evolution of the plastic deformation reduces the driving force of the transformation. On the other hand, a local plastic relaxation allows the accommodation of the strain caused by the MT and the nucleation and growth of the new martensitic variants. Finally, statistically stored dislocations are an irreversible structural change which affect the energy landscape by their own elastic fields. Thus, a general phase-field model for MT should include not only the driving forces originating from the elastic fields, but also the effects resulting from the plastic strain fields.

The plastic activity in the phase-field theory has already been treated by modeling the dislocations [14] and their dynamics [15,16,17,18,19]. A phase-field model of the evolution of a dislocation system based on the time depending Ginzburg-Landau (TDGL) equation was developed by Wang et al. [17]. At the same time, Koslowski et al. [19] formulated a phase-field theory of the dislocation dynamics for an arbitrary number and arrangement of dislocation lines based on energy minimization.

The plastic deformation can also be added to the phase-field model by introducing a plastic strain field defined at the mesoscale. A version of this approach has been recently proposed by Zhou et al. [20,21] where the plastic strain is related to the inter-dislocation distance. The evolution of the dislocation phase fields is described by the TDGL equation similar to the evolution of the martensitic phase fields. The difference to the individual dislocation dynamic models is that the model proposed by Zhou et al. describes the evolution of a dislocation mixture. Another version of this approach, which take into account the strain energy relaxation due to plastic accommodation, has been proposed by Yamanaka [22,23] based on the PFM theory and the elastoplastic PF model suggested by Guo et al. [24].

To describe the plastic deformation in single crystals many models use the crystal plasticity framework in which the evolution of plastic strain is described by means of an elastic driving force. It is the so called phenomenological viscoplastic approach [25,26,27,28,29]. Crystal plasticity methods developed by Ma and Roters [30,25,29] have recently made remarkable progress and allow the numerical study of deformation processes on the basis of thermally activated dislocation evolution. The model preserves the crystallographic features of dislocation slip processes and captures the commonly accepted concepts of dislocation processes in plastic deformation, especially various dislocation interaction processes as interactions of mobile and statistically stored dislocation, the formation of locks and dipoles or the thermal and athermal annihilation in a continuum dislocation density framework. The original concept [30] for fcc single crystals has been extended to polycrystals, considering grain boundary interactions and geometrically necessary dislocations as well as the extension to dislocations in bcc crystals [31,32,33,29,25]. It should be noted that a number of other works have been published recently which couple the phase-field simulation with crystal plasticity schemes at the mesoscale [34,35] and do not take into account the plastic accommodation caused directly by the solid-solid transformation.

Crystal plasticity models, their further developments based on microscopically interpretable state-variables and their evolution based on sound physical principles are very attractive for coupling with solid-solid phase transitions and offer new research directions and new insights into the mechanisms of martensitic phase transformations. One contribution in this direction is the work of Kundin et al. [36], where the crystal plasticity model [30,25,29] is coupled to the phase-field model of the MT that allows to resolve the dynamics of individual martensitic plates. It has been demonstrated that the formation of special martensite morphologies (butterfly type) in Fe-Ni is assisted by the formation of plastic strain fields in the austenitic matrix, which then are inherited by the growing martensitic plates as it was experimentally observed in the works [37]. The model also uses methods of earlier models for the simulation of transformation induced plasticity [39].

The main goal of the current paper is the understanding of the evolution of the dislocation during the MT and the interaction of the plastic strain with the transformation front. The kinetic of the MT is described by the elasto-plastic PF model of the MT. The dislocations are treated as a separate dislocation field and their evolution is treated using the model of thermally activated dislocation motion [30,25,29]. In our investigation we concentrate on the inheritance of the dislocations by the martensitic phase. The previous work in this direction is the paper of Ostwald et al. [40], where the dislocation inheritance is considered as a result of the interaction between phase-transformation and plasticity effects. The authors introduced a so-called plastic inheritance law, which describes the plastic strain evolution during the transformation front propagation. It was assumed that the dislocations neither generate nor annihilate on the transformation front, i.e. the overall amount of plastic deformations remains constant. The dislocations can be only inherited in a growing martensitic phase or pushed by the transformation front, increasing the plastic strain in the parent austenitic phase. An inheritance probability function was suggested for the quantitative description of the inheritance process, which is equal to the fraction of the inherited dislocation density. In contrast to this inheritance mechanism we proceed from the fact that there are no physical driving force to push dislocations from the transformation front. We consider the mechanism of the annihilation of the dislocations on the propagating martensitic front and the generation of the dislocations in the austenitic matrix. The probability of the dislocation inheritance is defined as the fraction of the remaining dislocation density after the annihilation.

We first start with recalling the phase-field microelasticity model of the MT extended by taking into account plastic strains in Section 2. The differential equation describing the evolution of plastic strain is presented in Sections 2.3. The coupling of phase-transformation and plasticity effects is incorporated in one algorithm. Details on the numerical investigation of the transformation front and the plastic strain are provided in Section 3, where the model is applied to a hypothetical Fe-Ni alloy. In addition, when various phase-field model parameters are applied, the resulting effect on the inheritance kinetics was predicted by the suggested model and compared with the reported data.

2 Theoretical part

2.1 The main parameters of the elasto-plastic phase-field model of MT

Following the concept developed in the PFM theory [5,7,6,13] we consider a coherent multi-phase mixture with the order parameters $\eta_p(\mathbf{r})$ and the local stress-free strain tensor $\varepsilon_{ij}^0(p, \mathbf{r}) = \varepsilon_{ij}^0(p)\eta_p(\mathbf{r})$ where p identifies a crystallo-

graphic variant. The order parameters are treated as phase-field variables so that $\eta_p \in [0, 1]$ and satisfy the property $\sum_{p=1}^{\nu} \eta_p(\mathbf{r}) = 1 - \phi_A(\mathbf{r})$ where $\phi_A(\mathbf{r})$ is the phase-field variable responsible for the presence of the austenite.

The dislocations are characterized by a Burgers vector $\mathbf{b}^{(\alpha)}$ and a slip plane with a normal $\mathbf{n}^{(\alpha)}$ defined by the crystallography of the austenitic (or martensitic) phase. Here, α is an index corresponding to a slip system. We use the symmetric Schmid tensor for a slip system α defined as $\hat{\mathbf{M}}^{(\alpha)} = \mathbf{n}^{(\alpha)} \otimes \mathbf{m}^{(\alpha)}$ where $\mathbf{m}^{(\alpha)} = \mathbf{b}^{(\alpha)}/b^{(\alpha)}$ is the unit vector in the direction of the Burgers vector, which expresses the slip direction. Then we define a dimensionless dislocation function through the dislocation densities of mobile, $\rho_{M,\alpha}$, and immobile, $\rho_{I,\alpha}$, dislocations

$$\phi_{\alpha}^d(\mathbf{r}) = b^{(\alpha)} \sqrt{\rho_{I,\alpha}(\mathbf{r}) + \rho_{M,\alpha}(\mathbf{r})} \quad (1)$$

as an analog of a phase-field variable. It is equal to the unity if the distance between the dislocations in the full volume is equal to the Burgers vector. The local stress-free plastic strain tensor caused by dislocations of an α -th slip system is given then by

$$\varepsilon_{ij}^d(\alpha, \mathbf{r}) = M_{ij}(\alpha) \phi_{\alpha}^d(\mathbf{r}). \quad (2)$$

Note that the sum of all dislocation functions is smaller than 1 $\sum_{\alpha=1}^{\mu} \phi_{\alpha}^d(\mathbf{r}) \leq 1$. We assume that ν is the number of the martensitic variants and μ is the number of the slip systems.

2.2 The evolution of the order parameters in the elasto-plastic phase-field model

The formulation of the total free energy of a system as a function of the order parameters is the key step in the development of phase-field models. In the standard phase-field formulation the total free energy is divided into three terms: the gradient energy term, the double well potential term (both terms are responsible for the interface energy) and the chemical free energy that provides the chemical driving force for the transformation. Concerning the MT, there are an additional elastic strain energy that suppresses or accelerates the transformation. The chemical free energy and the double well potential term in PFM theory of the MT are usually considered together and approximated by a Landau polynomial expansion with respect to the order parameters [50].

In the present study we reformulate the PFM theory in terms of the standard phase-field modeling [52,53]. The evolution of the order parameters in the system with the plastic strain is governed by the elasto-plastic phase-field kinetic equation

$$\begin{aligned}
\frac{1}{\mathcal{M}} \frac{\partial \eta_p(\mathbf{r})}{\partial t} = & K \nabla^2 \eta_p(\mathbf{r}) - H f'_{\eta_p} + \Delta f g'_{\eta_p} + \sigma_{ij}^{\text{appl}} \varepsilon_{ij}^0(p) g'_{\eta_p} \\
& - c_{ijkl} \varepsilon_{ij}^0(p) \left[\sum_{q=1}^{\nu} \varepsilon_{kl}^0(q) (\eta_q(\mathbf{r}) - \bar{\eta}_q) + \sum_{\beta=1}^{\mu} M_{kl}(\beta) (\phi_{\beta}^d(\mathbf{r}) - \bar{\phi}_{\beta}^d) \right] \\
& + \int c_{ijkl} \varepsilon_{kl}^0(p) e_i \Omega_{jm}(\mathbf{e}) \hat{\sigma}_{mn}^0(\mathbf{k}) e_n e^{i\mathbf{k} \cdot \mathbf{r}} \frac{d^3 \mathbf{k}}{(2\pi)^3},
\end{aligned} \tag{3}$$

where the Fourier transform of the stress is calculated by

$$\hat{\sigma}_{mn}^0(\mathbf{k}) = \int_V c_{mnjk} \left[\sum_{q=1}^{\nu} \varepsilon_{jk}^0(q) (\eta_q(\mathbf{r}) - \bar{\eta}_q) + \sum_{\beta=1}^{\mu} M_{jk}(\beta) (\phi_{\beta}^d(\mathbf{r}) - \bar{\phi}_{\beta}^d) \right] e^{-i\mathbf{k} \cdot \mathbf{r}} d^3 \mathbf{r}. \tag{4}$$

Here c_{ijkl} is the elastic modulus, Ω_{jm} is the Fourier transform of the Green function, $\bar{\eta}$ and $\bar{\phi}$ are the volume averaging functions, $\sigma_{ij}^{\text{appl}}$ is the applied stress.

The first term in the right hand side of eq. (3) is the gradient term, which forces interfaces to have a finite width. The second term is the double potential function and the third term is the driving force. Then \mathcal{M} is the mobility of the interface, $K = \frac{\gamma\xi}{a_1}$ is the gradient coefficient, $H = \frac{\gamma}{a_1\xi}$ is the coefficient before the double well function, ξ and γ are the interface width and the interface energy, respectively, which are assumed to be equal for all solid-solid interfaces.

The functions f'_{η_p} and g'_{η_p} are the derivatives of the model functions with respect to the chosen order parameter. The model function f is the double well potential and is defined as follows

$$f(\vec{\eta}) = \sum_{q=1}^{\nu} \eta_q^2 - 2 \sum_{q=1}^{\nu} \eta_q^3 + \left(\sum_{q=1}^{\nu} \eta_q^2 \right)^2. \tag{5}$$

The function g is responsible for the chemical driving force and defined as

$$g(\vec{\eta}) = 4 \sum_{q=1}^{\nu} \eta_q^3 - 3 \left(\sum_{q=1}^{\nu} \eta_q^2 \right)^2. \tag{6}$$

These model functions serve the goal to keep the order parameters between 0 and 1. In Appendix A we show that the chosen model functions satisfy the properties of the standard phase-field model and derive their relation to the Landau polynomial expansion usually used in PFM theory.

The undercooling responsible for the chemical driving force is given by

$$\Delta f = Q_M (T_M - T) / T_M, \tag{7}$$

where Q_M and T_M are the latent heat and T is the temperature of the MT, respectively.

2.3 The evolution of the plastic strain

In this section we describe the time evolution of the dislocation density generated during the MT and forming plastic deformation strain. The dislocation density will first evolve in the austenitic phase. Then, due to the interaction of the plastic strain with the transformation front, one part of the dislocations will cross the interface without or with small changes of the slip system and be inherited in the martensite. The other part of the dislocation will annihilate by the interaction with the dislocations of the same slip system collected at the transformation front. The kinetics of these processes depends on the growth velocity of the transformation front and the resistance stress of the matrix. It should also be taken into account that a part of the dislocations can annihilate in the bulk phase. In the following we consider a single crystal system, i.e. a system which contains only one grain without boundaries.

In order to simulate the evolution of the dislocation density and thereby the dislocation function, we define additionally to the mobile and immobile dislocations the parallel dislocation density $\rho_{P,\alpha}$ and the forest dislocation density $\rho_{F,\alpha}$ for a slip system α following [30] as

$$\rho_{M,\alpha} = \frac{2k_B T}{c_1 c_2 c_3 G b_\alpha^3} \sqrt{\rho_{F,\alpha} \rho_{P,\alpha}}, \quad (8)$$

$$\rho_{P,\alpha} = \sum_{\beta=1}^{\mu} \rho_{I,\beta} \left| \sin \left(\mathbf{n}^{(\alpha)}, \mathbf{n}^{(\beta)} \times \mathbf{m}^{(\beta)} \right) \right|, \quad (9)$$

$$\rho_{F,\alpha} = \sum_{\beta=1}^{\mu} \rho_{I,\beta} \left| \cos \left(\mathbf{n}^{(\alpha)}, \mathbf{n}^{(\beta)} \times \mathbf{m}^{(\beta)} \right) \right|, \quad (10)$$

where G is the shear modulus, k_B is the Boltzmann constant, T is the temperature and c_1, c_2, c_3 are material constants.

Following the theory presented in [25,30] we calculate the evolution of the immobile dislocation density as

$$\begin{aligned} \dot{\rho}_{I,\alpha} = & c_4 \sqrt{\rho_{F,\alpha}} \dot{\gamma}_\alpha - c_5 \rho_{I,\alpha} \dot{\gamma}_\alpha - c_7 \exp \left(-\frac{Q_{\text{bulk}}}{k_B T} \right) \frac{|\tau_\alpha|}{k_B T} (\rho_{I,\alpha})^2 \dot{\gamma}_\alpha^{c_8} \\ & - c_9 \rho_{I,\alpha} \sum_{p=1}^{\mu} \dot{\gamma}_p + c_{10} \phi_A \nabla [\mathbf{n}_\alpha \times \nabla] \rho_{I,\alpha}, \end{aligned} \quad (11)$$

where $\dot{\gamma}_\alpha$ is the plastic shear rate, Q_{bulk} is the activation energy for climb and τ_α is the external stress.

Eq. (11) combines three processes in the bulk phase: immobilization of the mobile dislocations, non-thermal annihilation with the immobile dislocations of the same slip system and thermal annihilation by climb of edge dislocations with material constants c_4 , c_5 and c_7 , respectively. The probability of these processes are governed by the plastic shear rate $\dot{\gamma}_\alpha$.

Furthermore, we propose to take into account an additional process of the non-thermal annihilation at the martensitic transformation front with a constant c_9 . The probability of this process is proportional to the local dislocation density and the velocity of the MT front, which is related to the evolution of the order parameter $\dot{\eta}_p$. Physical meaning of this term is that the transformation front collect the dislocations, which can later annihilate with the dislocations of the same slip system during the front propagation. The increasing collection or striking of the dislocations on the front should increase with the increasing transformation rate, because the system has less time to relax. In the following we will call the annihilation at the MT front as the annihilation term. In this study the two cases are considered with and without the annihilation term. Note that the parameter c_9 is a phenomenological parameter, which should be found experimentally. In the simulation it is chosen of five time smaller than the parameter c_5 , which is responsible for the annihilation in the bulk phase.

Similar to the gradient energy formulation used in the phase-field model of individual dislocations [17], the gradient of the dislocation density $\rho_{I,\alpha}$ is added to the elastic energy of the dislocation and subsequently the Laplace term is added to the evolution equation (11). This gradient can be attributed to the core energy of the dislocations. The coefficient c_{10} has to guarantee a smooth transition of the deformation strain field profile across the sheared non-sheared martensite-austenite boundaries. The value of c_{10} should be the same order as the square of the dislocation core size. A similar term was used in work [21] for the simulation of the γ' -coarsening in the presence of the dislocation field and is reasonable.

The plastic shear rate can be defined according to the Orowan equation as

$$\dot{\gamma}_\alpha = \phi_A \rho_{M,\alpha} b_\alpha v_\alpha, \quad (12)$$

where we assume that the plastic deformation is hindered in the martensite due to much higher flow stresses compared to the austenite. We describe the evolution of plastic slip during the process only in the austenitic phase and multiply the plastic shear rate with ϕ_A .

The average dislocation velocity v_α based on the model of thermally activated

dislocation motion can be found as [30,25,29]

$$v_\alpha = \lambda_\alpha \nu_\alpha \exp\left(-\frac{Q_{\text{slip}}^\alpha}{k_B T}\right) \exp\left(\frac{|\tau^\alpha| - \tau_{\text{pass}}^\alpha}{k_B T} V_\alpha\right), \text{ for } |\tau^\alpha| > \tau_{\text{pass}}^\alpha, \quad (13)$$

where $\tau_{\text{pass}}^\alpha = c_1 G b_\alpha \sqrt{\rho_{P,\alpha} + \rho_{M,\alpha}}$ is the passing stress of the mobile dislocations, ν_α is the attack frequency, $Q_{\text{slip}}^\alpha = G b_\alpha^3 / 2$ is the effective activation energy for the dislocation slip, $\lambda_\alpha = \frac{c_2}{\sqrt{\rho_{F,\alpha}}}$ is the jump width and $V_\alpha = c_3 b_\alpha^2 \lambda_\alpha$ is the activation volume, where c_1 , c_2 and c_3 are material constants.

In the simulations numerical problems arise with eq. (13) due to the very strong exponential function of the stress. For numerical reasons we prefer an alternative variant of the evolution equation according to a Norton type flow rule

$$v_\alpha = \lambda_\alpha \nu_\alpha \exp\left(-\frac{Q_{\text{slip}}^\alpha}{k_B T}\right) \left(\frac{|\tau^\alpha| - \tau_{\text{pass}}^\alpha}{\tau_{\text{cut}}}\right)^n, \quad (14)$$

where $\tau_{\text{cut}} = 0.2$ GPa and $n = 5$ for cubic systems. This type of equation was used in [34] to study rafting in Ni-based superalloys.

The external stress τ^α , which is the driving force of the dislocation evolution, is caused by the applied force, growing martensitic phases and dislocation fields. It can be derived from the total elastic energy as

$$\begin{aligned} \tau_\alpha = & -c_{ijkl} M_{ij}(\alpha) \left[\sum_{q=1}^{\nu} \varepsilon_{kl}^0(q) (\eta_q - \bar{\eta}_q) + \sum_{\beta=1}^{\mu} M_{kl}(\beta) (\phi_\beta^d - \bar{\phi}_\beta^d) \right] \\ & + \int_{\hat{V}} c_{ijkl} M_{kl}(\alpha) e_i \Omega_{jm}(\mathbf{e}) \hat{\sigma}_{mn}^0(\mathbf{k}) e_n e^{(i\mathbf{k} \cdot \mathbf{r})} \frac{d^3 \mathbf{k}}{(2\pi)^3} + \sigma_{ij}^{\text{appl}} M_{ij}(\alpha), \end{aligned} \quad (15)$$

where the Fourier transform of the stress $\hat{\sigma}_{mn}^0(\mathbf{k})$ is defined by (4).

The set of equations (8) - (12), (14), (15) are calculated in each step of the simulation for all slip systems, then the dislocation functions are defined according to eq. (1) and inserted in the kinetic equation (3).

3 Numerical simulation

3.1 Choice of parameters

For the numerical investigation we chose a hypothetical Fe-30%Ni alloy, where the occurring lenticular-type martensite is characterized by the mixture of twinning and dislocation structure.

Table 1
Material and processing parameters used in the simulation

Parameter	Value
Temperature of MT	$T_M = 400$ K
Interface energy	$\gamma = 1.9 \times 10^{-2}$ J m ⁻² [51]
Latent heat	$Q_M = 3.5 \times 10^8$ J m ⁻³ [7]
Pre-deforming	$\rho_I = 10^{12}$ m ⁻²
External applied stress	$\sigma_{11}^{\text{appl}} = \sigma_{33}^{\text{appl}} = -1$ GPa
Shear modulus	$G = 28$ GPa
Poisson coefficient	$\nu = 0.374$
Material constants	$c_1 = 0.18$ $c_2 = 5.0$ $c_3 = 5.0$ $c_4 = 8.0 \cdot 10^6$ m ⁻¹ $c_5 = 10$ $c_7 = 1 \times 10^7$ m ⁵ s ^{c8} $c_8 = 0.3$ $c_9 = 2$ $c_{10} = 0.1 l_0^2$
Attack frequency	$\nu_0 = 10^{10}$ s ⁻¹
Activation energy	$Q_{\text{slip}} = 2.3 \times 10^{-19}$ J
Activation energy	$Q_{\text{bulk}} = 2.4 \times 10^{-19}$ J
Lattice constant	$a_0 = 3.59 \times 10^{-10}$ m

The material parameters and phase-field model parameters used in the simulations are listed in Tables 1, 2.

The reason of the choice of the discretization size is that we first chose the relation between the interface width and the maximal capillary length $d_0 = \gamma/(a_1 E_0) = 1.3 \times 10^{-11}$ m. That implies that $\xi/d_0 < 200$, which is a requirement of the asymptotic limit in the phase-field model [53]. In the simulations we used the phase-field equations in dimensionless form by measuring length in units l_0 , time in units of τ_0 (it can be estimated from the experimental formation rate for the MT of order 10^{-7} s) and the energy in units of E_0 , which is the typical strain energy of MT. Then the mobility of the interface is calculated as $\mathcal{M} = 1/(\tau E_0)$.

Table 2

Phase-field model parameters used in the simulation

Parameter	Value	Units
Length scale, l_0	1.3×10^{-9}	m
Time scale, τ_0	3.3×10^{-10}	s
Energy scale, E_0	3.07×10^9	J m ⁻³
Discretization size, Δx	1	l_0
Time step, Δt	0.125	τ_0
Interface width, ξ	1.5	l_0
Gradient coefficient, K	0.0152	$E_0 l_0^2$
Double-well potential coefficient, H	0.0067	E_0
Landau energy parameter, a_2	0.0134	E_0
Interface mobility, \mathcal{M}	1	$(\tau_0 E_0)^{-1}$
Undercooling, Δf	0.06	E_0

For these parameters the Landau energy parameter $a_2 = 2\gamma/(a_1\xi)$ in the chemical energy function (see Appendix A) equals to $a_2 = 0.0134 E_0$. The estimation of the gradient coefficient in eq. (3) yields $K = \gamma\xi/(a_1) = 0.0152 E_0 l_0^2$. For the comparison with work [13] the gradient coefficient is in the same order ($K = 0.01624 E_0 l_0^2$) but the Landau energy parameter is ten times larger ($a_2 = 0.312 E_0$). The interface width used in the simulation was very much smaller than the chosen discretization size $\xi = \sqrt{K/H} = 0.32 l_0$. This means that the increasing parameter a_2 results in a decreasing interface width. In the simulation we used the parameters listed in Table 1. For comparison we also carried out the simulations with $a_2 = 0.312 E_0$ ($\xi = 0.32 l_0$) to show the influence of this parameter on the annihilation term.

For three variants of the MT we used the Bain transformation matrices:

$$\begin{aligned}
\varepsilon_{11} &= 0.1322, \varepsilon_{22} = 0.1322, \varepsilon_{33} = -0.1994, \text{ variant 1;} \\
\varepsilon_{11} &= -0.1994, \varepsilon_{22} = 0.1322, \varepsilon_{33} = 0.1322, \text{ variant 2;} \\
\varepsilon_{11} &= 0.1322, \varepsilon_{22} = -0.1994, \varepsilon_{33} = 0.1322, \text{ variant 3.}
\end{aligned}$$

In the fcc lattice of the austenitic matrix 24 variants of the dislocation slip were chosen with slip planes of type $\{111\}_A$ and slip directions of type $\langle 101 \rangle_A$. For the calculation of the Burgers vector we used $b = a_0/\sqrt{2}$, where a_0 is the lattice constant.

3.2 Numerical investigation of the dislocation inheritance

In this section we present the simulation results for the case where dislocations exist in the pre-deformed austenite. A nucleus containing 3 martensitic variants is generated in a system of size $38 \times 38 \times 38 \Delta x$ and $64 \times 64 \times 64 \Delta x$, respectively. Periodic boundary conditions are applied to the systems for all fields.

An external force of 1 GPa is imposed in direction $[\bar{1}0\bar{1}]$. This force suppresses one martensitic variant and promotes two other variants (variants 1 and 2), which produce a twinning structure. The dislocation density evolves during the simulation due to the applied stress and the stress from the MT.

The probability of dislocation inheritance from the austenitic matrix to the martensitic phase is defined as a ratio between the averaged dislocation density with and without the annihilation term in eq. (11)

$$\mathcal{P}_\alpha(t) = \frac{\bar{\rho}_{I,\alpha} + \bar{\dot{\rho}}_{I,\alpha} dt}{\bar{\rho}_{I,\alpha} + \bar{\dot{\rho}}_{I,\alpha} dt + \overline{c_9 \rho_{I,\alpha} \dot{\eta}} dt}, \quad (16)$$

where $\dot{\eta} = \sum_{p=1}^{\mu} \dot{\eta}_p$ and \bar{x} identify a space averaged variable over the interface between martensitic and austenitic phases

$$\bar{x} = \frac{\int_0^{V_{box}} x \eta \phi_A dV}{\int_0^{V_{box}} \eta \phi_A dV}. \quad (17)$$

Thus, we consider only the dislocations which can take part in the annihilation process at the MT front. Note that from the probability $\mathcal{P}_\alpha(t)$ the contribution of the annihilation term to the total dislocation density is derived as $1 - \mathcal{P}_\alpha(t)$.

During the simulation we additionally control the ratio between the mean dislocation densities in the martensite (all variants) and austenite

$$\mathcal{R}_\alpha(t) = \frac{\bar{\rho}_{I,\alpha}|_M}{\bar{\rho}_{I,\alpha}|_A}. \quad (18)$$

The simulated microstructure during the MT at 1500, 2500 and 5000 time steps is shown in Figs. 1-3 for three cases. In the first and second tests (Figs. 1 and 2) we simulated the microstructure with the interface width $\xi = 1.5 l_0$ in boxes of size $38 \Delta x$ and $64 \Delta x$. The microstructure consists of twinned martensitic plates, which belong to one martensitic lath. The size of the system influences the number and the thickness of the growing plates. It can be seen that for the smaller system size the number of the martensitic plates is larger and their thickness is evenly distributed in the volume. For the smaller system size the thickness of martensitic plates becomes 2-3 times larger at the end of

the growth. In the third test (Fig. 3) the interface width was chosen $\xi = 0.32 l_0$. Furthermore the coordinate system was rotated to $[\bar{1}\bar{1}2], [111], [\bar{1}10]$. In the simulation box of size $64 \Delta x \times 6$ nuclei of the martensitic phase were inserted randomly with the mean time interval equal to 100 time steps. One nucleus grows in one martensitic lath, which consist of the thin twinned martensitic plates. The simulation test shows that for the small interface width $\xi = 0.32 l_0$ the MT can not be completed at the chosen undercooling. To reach the full martensitic transformation the simulation was carried out at the increasing undercooling from Δf to $3\Delta f$ for 2500 simulation time steps that corresponds to the cooling rate $2 \cdot 10^8$ K/s.

The 2D sections ($x - y$ -directions) of the microstructure and the dislocation density field (in logarithmic coordinates) are presented in Figs. 4 and 5 for the first and second test, respectively. It can be seen that the dislocation density increases first near the transformation front in the earlier stages of MT and strongly increases in the full austenitic volume at the end of the MT. The annihilation decreases the dislocation density in the martensitic phase (last column in Figs. 4,5).

For the analysis we chose two slip systems as examples of low and high interaction stresses between the martensite and the dislocation field. As a characteristic parameter of this interaction a maximum interaction stress can be proposed defined as

$$\tau_{\text{inter}}(\alpha, p) = c_{ijkl} M_{ij}(\alpha) \varepsilon_{kl}^0(p), \quad (19)$$

which influences the kinetics of the MT and the evolution of the dislocation field due to the phase transformation (see eq. 15). It is obviously that the interaction stress between the martensitic plates and the dislocation field depends on the orientation relationship between the corresponding martensitic variants and the dislocation slip systems. The full list of the interaction stresses between 12 slip systems and two martensitic variants is presented in Table 3. As an example for the visualization and the qualitative analysis we chose two typical slip systems which have different summary interaction stresses (see last column of Table 3). It is also remarkable that the evolution of the dislocations is faster in the martensitic variant 2 as in variant 1, because the interaction stress is not zero for both chosen slip systems. In Figs. 4,5 the difference between the diffusion fields in the areas of both martensitic variants can be seen, which is large in the variant 2 (yellow color).

The evolution of the mean dislocation density during the simulation is plotted in Fig. 6 (a,b) for two slip systems. It can be observed that the dislocation density in the martensite increases stronger without than with annihilation. It is obviously that the annihilation decreases the dislocation density in the martensite according to eq. (11). For the slip system 1 the dislocation density is larger due to the larger summary interaction stress.

Table 3

Interaction stress between the dislocation slip systems and mertensitic variants. The slip systems used in the simulation are underlined.

Slip system	Mart. variant 1	Mart. variant 2	sum
<u>(111)[$\bar{1}10$]</u> (1)	0	0.0736807	0.0736807
(11 $\bar{1}$)[$\bar{1}10$]	0	0.0736807	0.0736807
(111)[0 $\bar{1}1$]	-0.0736807	0	-0.0736807
($\bar{1}11$)[0 $\bar{1}1$]	-0.0736807	0	-0.0736807
(111)[10 $\bar{1}$]	0.0736807	-0.0736807	0
(1 $\bar{1}1$)[10 $\bar{1}$]	0.0736807	-0.0736807	0
($\bar{1}11$)[$\bar{1}\bar{1}0$]	0	-0.0736807	-0.0736807
(1 $\bar{1}1$)[$\bar{1}\bar{1}0$]	0	0.0736807	0.0736807
<u>($\bar{1}11$)[101]</u> (2)	-0.0736807	0.0736807	0
(11 $\bar{1}$)[101]	0.0736807	-0.0736807	0
(1 $\bar{1}1$)[0 $\bar{1}\bar{1}$]	0.0736807	0	0.0736807
(11 $\bar{1}$)[0 $\bar{1}\bar{1}$]	-0.0736807	0	-0.0736807

The time evolution of the probability of the inheritance, \mathcal{P}_α , is plotted in Fig. 7 (a). A comparison with Fig. 6 shows that the larger the dislocation density and their evolution rate, the larger the probability \mathcal{P}_α . The simulation with the small interface width $\xi = 0.32 l_0$ shows that the annihilation of the dislocations at the transformation front is very small. Indeed in this case the phase-field model gives maximal 2 discretization points on the interface, while for $\xi = 1.5 l_0$ the phase-field model gives minimal 4 discretization points. It is obviously that for a thicker interface the annihilation processes are more intensive.

The probability \mathcal{P}_α as function of the martensitic fraction is plotted in Fig. 7 (b). It slightly decreases for a long time and then strongly decreases at the middle of the MT due to the dislocation evolution in the austenite caused by the MT. At the end of the transformation the probability strongly increases to 1 for the system size $38 \Delta x$. That means that the annihilation of the dislocations at the interface increases with the increasing dislocation density and decreases with the decreasing transformation rate. For the system size $64 \Delta x$ \mathcal{P}_α is smaller than for the system size $38 \Delta x$ and it does not reach 1 at the end of the transformation. It can be explained by the fact that for the larger system size and correspondingly larger distance between the martensitic nucleus the content of the retained austenite is larger and the dislocation density is smaller (see Fig 6).

In Fig. 7 it can be also seen that for the slip system 1 the average probability of the inheritance is higher than for system 2. This can be explained by the higher interaction stress that causes the intensive dislocation density evolution and the corresponding decrease of the contribution of the annihilation term.

In the work [40] a convex inheritance probability function was proposed, where it was required to match the inheritance probability function to 0 at $x = 0$ and to 1 at $x = 1$. It was also assumed that if x tends to zero, the dislocation density in the austenite takes high values and forces to be inherited by the MT front. To proof the proposed convex inheritance probability function we found that the curves in Fig. 7 (b) can be approximated in their increasing part by a function of the martensitic fraction, x , similar to the proposed

$$\mathcal{P}_\alpha = k_0 + (1 - k_0)x \exp\left(-\frac{(1 - x)}{k_1 x}\right), \quad (20)$$

where k_0 is a minimal probability and k_1 is a hardening coefficient. For $x = 1$ the probability becomes 1. The value $k_1 x$ is responsible for the increasing plastic strain in the retained austenite due to the MT. For the simulated curves of the system size $38 \Delta x$ the parameters of eq. (20) are the following: $k_0 = 0.9710, 0.9490$ and $k_1 = 0.012, 0.010$ for the slip systems 1 and 2, respectively. For the system size $64 \Delta x$ the dependencies in Fig. 7 (b) can not be approximated by the chosen function.

The time dependency of the ratio between the dislocation densities in the martensite and austenite is plotted in Fig. 8 for two slip systems. The behavior is similar to the probability of the inheritance. With increasing dislocation density in the austenite the ratio \mathcal{R} decreases. The annihilation term decreases the dislocation density in the martensite at the earlier stages and does not influence the further evolution. It is interesting that without annihilation the dislocation density is higher in the martensite and the ratio \mathcal{R} is higher than 1 all the time during the MT.

The comparison of the kinetics of the MT with and without dislocation evolution and with and without annihilation term is shown in Fig. 9. The generation of the dislocation during the MT increases the rate of the MT and the final martensitic fraction. The annihilation on the contrary decreases the transformation rate. It can be seen that for small system size $38 \Delta x$ the final martensitic fraction also decreases with the annihilation term.

From the simulation results it follows that the contribution of the annihilation at the transformation front is smaller than 6%. That means that the contribution of the annihilation in the total process of the evolution of the plastic strain should be very small. But in spite of this the influence of the annihilation on the MT is essential. It is expressed in a decreasing rate of the MT

and a decreasing final martensitic fraction. And in addition the annihilation decreases the dislocation density in the martensitic phase almost to half.

4 Conclusions

In the present study the interaction of the MT front with the plastic strain in a Fe-Ni alloy has been investigated in detail by means of the elasto-plastic phase-field model.

The model takes into account the formation of accommodation dislocations in the austenitic matrix and the annihilation of the dislocations at the growing martensitic transformation front. It resolves the effects of the dislocation dynamics on the kinetics of the MT. It is found that the part of the dislocations inherited in the martensite can be defined as functions of the martensitic fraction and the plastic strain or the dislocation density in the austenitic matrix. As result of the numerical simulations the following phenomenological dependencies for the probability of the inheritance of the dislocations by the martensite are found:

- 1) \mathcal{P}_α depends on the plastic strain, the plastic shear rate and the transformation rate;
- 2) \mathcal{P}_α depends on the orientation relationship between the martensitic variants and dislocation slip systems;
- 3) \mathcal{P}_α depends on the mean distance between the nuclei of the martensitic phase;
- 4) \mathcal{P}_α can be describe as a function of the martensitic fraction.

Moreover, from our simulation follows the dependency of the probability of the dislocation evolution and the inheritance on the orientation relationship between the martensitic variants and dislocation slip systems.

5 Acknowledgement

Appendix A: The chemical energy function

The model function f is defined as follows

$$f(\vec{\eta}) = \sum_{q=1}^{\nu} \eta_q^2 - 2 \sum_{q=1}^{\nu} \eta_q^3 + \left(\sum_{q=1}^{\nu} \eta_q^2 \right)^2 \quad (.1)$$

and its derivative is equal to

$$f'_{\eta_p} = 2 \left(\eta_p - 3\eta_p^2 + 2\eta_p \sum_{q=1}^{\nu} \eta_q^2 \right). \quad (.2)$$

f reduces in the case of one martensitic variant to the standard double well function

$$f = \eta^2(1 - \eta)^2 \quad (.3)$$

with

$$f'_\eta = 2\eta(1 - \eta)(1 - 2\eta). \quad (.4)$$

For this function the numeric constant $a_1 = \sqrt{2}/3$ [53].

The model function g is defined as

$$g(\vec{\eta}) = 12 \left(\frac{1}{3} \sum_{q=1}^{\nu} \eta_q^3 - \frac{1}{4} \left(\sum_{q=1}^{\nu} \eta_q^2 \right)^2 \right) \quad (.5)$$

with a derivative

$$g'_{\eta_p} = 12 \left(\eta_p^2 - \eta_p \sum_{q=1}^{\nu} \eta_q^2 \right). \quad (.6)$$

Further g reduces in the case of the one martensitic variant to the model function

$$g = 12 \left(\frac{\eta^3}{3} - \frac{\eta^4}{4} \right) \quad (.7)$$

with

$$g'_\eta = 12\eta^2(1 - \eta). \quad (.8)$$

It can be seen that the second and third terms in the kinetic eq. (3) build together the well known Landau-type polynomial

$$\begin{aligned}
f_L &= Hf(\vec{\eta}) - \Delta f g(\vec{\eta}) \\
&= \frac{1}{2}a_2 \sum_{q=1}^{\nu} \eta_q^2 - \frac{1}{3}(3a_2 + 12\Delta f) \sum_{q=1}^{\nu} \eta_q^3 + \frac{1}{4}(2a_2 + 12\Delta f) \left(\sum_{q=1}^{\nu} \eta_q^2 \right)^2 \quad (.9)
\end{aligned}$$

where the Landau energy parameter $a_2 = 2H = \frac{2\gamma}{a_1\xi}$ is related to the nucleation barrier.

References

- [1] J. Dadda, H.J. Maier, D. Niklasch, I. Karaman, H.E. Karaca, Y. I. Chumlyakov, Metall. Mater. Trans. A **39** 2026–2039 (2008).
- [2] O. Graessell, L. Krueger, G. Frommeyer, L.W. Meyer, Int. J. Plasticity **16** 1391–1409 (2000).
- [3] K. Otsuka and C.M. Wayman. Shape Memory Materials. Cambridge University Press, 1999.
- [4] A. G. Khachaturyan, Theory of structural transformations in solids, John Wiley & Sons Ltd., New York, (1986).
- [5] Y. Wang and A.G. Khachaturyan, Acta Mater. **45** 759–773 (1997).
- [6] Y. M. Jin, A. Artemev and A. G. Khachaturyan, Acta Mater. **49** 2309–2320 (2001).
- [7] A. Artemev, Y.M. Jin and A.G. Khachaturyan, Acta Mater. **49** 1165–1177 (2001).
- [8] A. Artemev, Y.M. Jin and A.G. Khachaturyan, Philos. Mag. A **82** 1249–1270 (2002).
- [9] Y. Wang, L.Q. Chen, A.G. Khachaturyan, in: W.C. Johnson, J.M. Howe, D.E. Laughlin, W.A. Soffa (Eds.), Solid-Solid Phase Transformations, TMS, Warrendale, PA, USA, 1994, pp. 245265.
- [10] Y. Wang, L.Q. Chen, in: E.N. Kaufmann (Ed.), Methods in Materials Research, A Current Protocols, John Wiley & Sons, Inc., 2000, pp. 2a.3.12a.3.23.
- [11] L.Q. Chen, Annu. Rev. Mater. Res. **32** (2002) 113140.
- [12] C. Shen, Y. Wang, in: S. Yip (Ed.), Handbook of Materials Modeling, Part B: Models, Springer, New York, 2005, pp. 2117–2142.
- [13] W. Zhang, Y.M. Jin, A.G. Khachaturyan, Acta Mater. **55** 565–574 (2007)
- [14] S.Y. Hu and L.Q. Chen, Acta Mater. **49(3)** 463–472 (2001).
- [15] D Rodney, A Finel MPS Symp. Proc. **652** Y4 (2001).

- [16] D Rodney, Y. Le Bouar, A. Finel, *Acta Mater.* **51** 17 (2003).
- [17] Y.U. Wang, Y.M. Jin, A. M. Cuitino and A.G. Khachaturyan, *Acta Mater.* **49** 1847-1857 (2001).
- [18] N. Zhou, C. Shen, M.J. Mills, Y. Wang, *Acta Mater.* **55** 5369 (2007).
- [19] M. Koslowski, A. M. Cuitino and M. Ortiz, *J. Mech. Phys. Solids* **50** 2597–2635 (2002).
- [20] N. Zhou, C. Shen, M.J. Mills, Y. Wang, *Acta Mater.* **56** 6156 (2008).
- [21] N. Zhou, C. Shen, M.J. Mills, Y. Wang, *Phil. Mag.* **90** 405–436 (2010).
- [22] A. Yamanaka, T. Takaki, Y. Tomita APCOM07 in conjunction with EPMESC XI, December 3-6, 2007, Kyoto, JAPAN.
- [23] A. Yamanaka, T. Takaki, Y. Tomita, M. Yoshino, *Proceedings of X International Conference on Computational Plasticity - COMPLAS X (CD-ROM)* **462** 1-4 (2009).
- [24] X. H. Guo, S-Q. Shi, X. Q. Ma, *Appl. Phys. Lett.* **87** 221910 (2005).
- [25] F. Roters, D. Raabe, G. Gottstein, *Acta Mater.* **48** 4181–4189 (2000).
- [26] J.W. Hutchinson, *Proc. Roy. Soc. London A* **319** 247–272 (1970).
- [27] J.R. Rice, *J. Mech. Phys. Solids* **19** 433–455 (1971).
- [28] R.J. Asaro, A. Needleman, *Acta Mater.* **33** 923 (1985).
- [29] F. Roters, P. Eisenlohr, L. Hantcherli, D.D. Tjahjanto, T.R. Bieler, D. Raabe, *Acta Materialia* **58** 1152–1211 (2010).
- [30] A. Ma and F. Roters, *Acta Mater.* **52** 3603–3612 (2004).
- [31] A. Ma, F. Roters, D. Raabe, *Acta Mater.* **54** 2169–2179 (2006).
- [32] A. Ma, F. Roters, D. Raabe, *Acta Mater.* **54** 2181–2194 (2006).
- [33] A. Ma, F. Roters, D. Raabe, *Comp. Mat. Sci* **39** 91–95 (2007).
- [34] A. Gaubert, Y. Le Bouar and A. Finel, *Phil. Mag.* **90** 375–404 (2010).
- [35] T. Takaki, Y. Tomita, *Intern. J. Mech. Sci.* **52** 320–328 (2010).
- [36] J. Kundin, D. Raabe, H. Emmerich, *J. Mech. and Phys. Solids* **59** 2082–2102 (2011).
- [37] E. K. H. Salje, H. Zhang, H. Idrissi, D. Schryvers, M. A. Carpenter, X. Moya, and A. Planes, *Phys. Rev. B* **80** 134114 (2009).
- [38] H. Sato, S. Zaeferrer, *Acta Mater.* **57** 1931-1937 (2009).
- [39] D.D. Tjahjanto, S. Turteltaub, A.S.J. Suiker, *Cont. Mech. Thermodyn.* **19** 399 (2008).

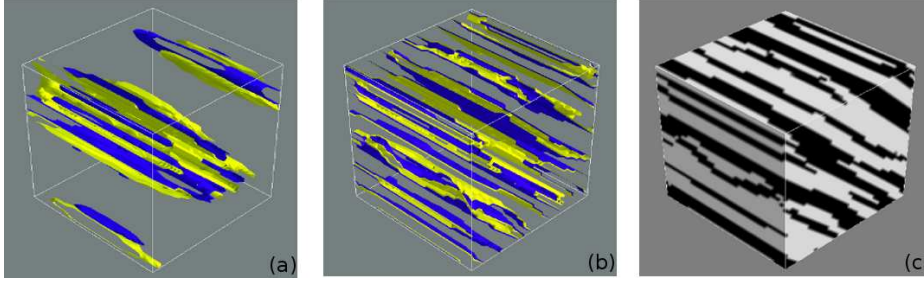


Fig. .1. 3D images of simulated microstructures during MT for the box of size $38 \Delta x$ with $\xi = 1.5 l_0$ at 1500(a) and 2500 (b) time steps; the surface view at 2500 time steps (c).

- [40] R. Ostwald, T. Bartel, A. Menzel, Int. J. Structural Changes in Solids – Mechanics and Applications **3(1)** 63-82 (2011).
- [41] L.Q. Chen, Y. Wang and A.G. Khachaturyan, Phil. Mag. Lett. 65 (1992) p.15–23.
- [42] C. Shen and Y. Wang, Acta mater. **51** 2595–2610 (2003).
- [43] C. Shen and Y. Wang, Acta mater. **52** 683–691 (2004).
- [44] J.F. Breedis, and C.M. Wayman, Trans. AIME, **224** 1128 (1962).
- [45] H.K.D.H. Bhadeshia, Worked Examples in the Geometry of Crystals, 2nd edition. Institute of Materials, London, 2001.
- [46] M. Umemoto, I. Tamura, J. Phys. Colloques **43** 523 (1982).
- [47] M. Umemoto, E. Yoshitake, I. Tamura, J. Mater. Sci. **18** 2893 (1983).
- [48] R.L. Patterson, and C.M. Wayman, Acta Metall. **14** 3437 (1966).
- [49] S. Turteltaub, A.S.J. Suiker, Intern. J. Solids and Structures **43** 4509 (2006).
- [50] P. Toledano, V. Dmitriev, Reconstructive Phase Transitions, World Scientific, New Jersey, 1996.
- [51] V.M. Kuznetsov, R.I. Kadyrov, G.E. Rudenskii, J. Mater.Sci. Technol. **14** 320 (1998).
- [52] G. Caginalp, Phys Rev. A **39** 5887 (1989).
- [53] A. Karma and W. J. Rappel, Phys. Rev. E **57** 4323 (1998).

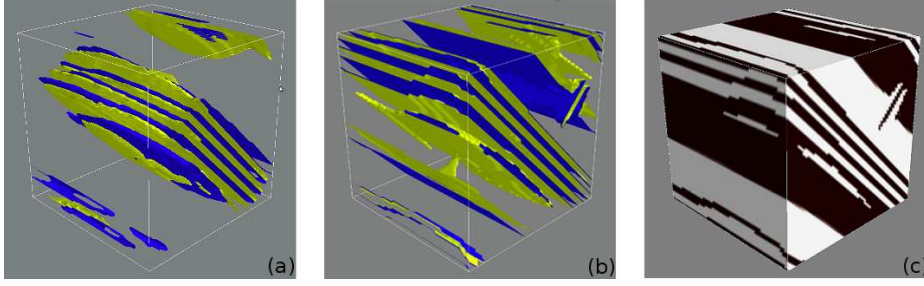


Fig. .2. 3D images of simulated microstructures during MT for the box of size $64 \Delta x$ with $\xi = 1.5 l_0$ at 2500 (a) and 5000 (b) time steps; the surface view at 5000 time steps (c).

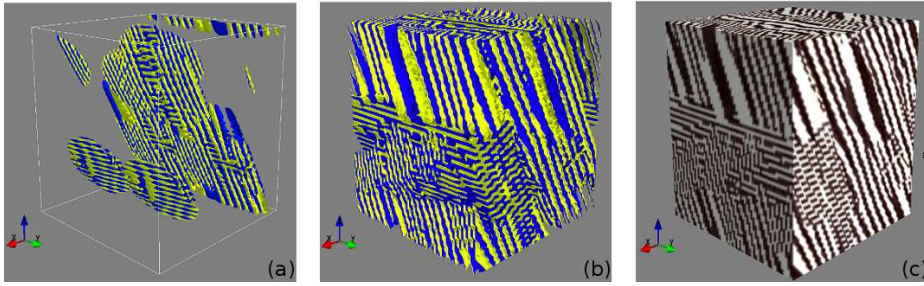


Fig. .3. 3D images of simulated microstructures during MT for the box of size $64 \Delta x$ with $\xi = 0.32 l_0$ at 2500 (a) and 5000 (b) time steps; the surface view at 5000 time steps (c).

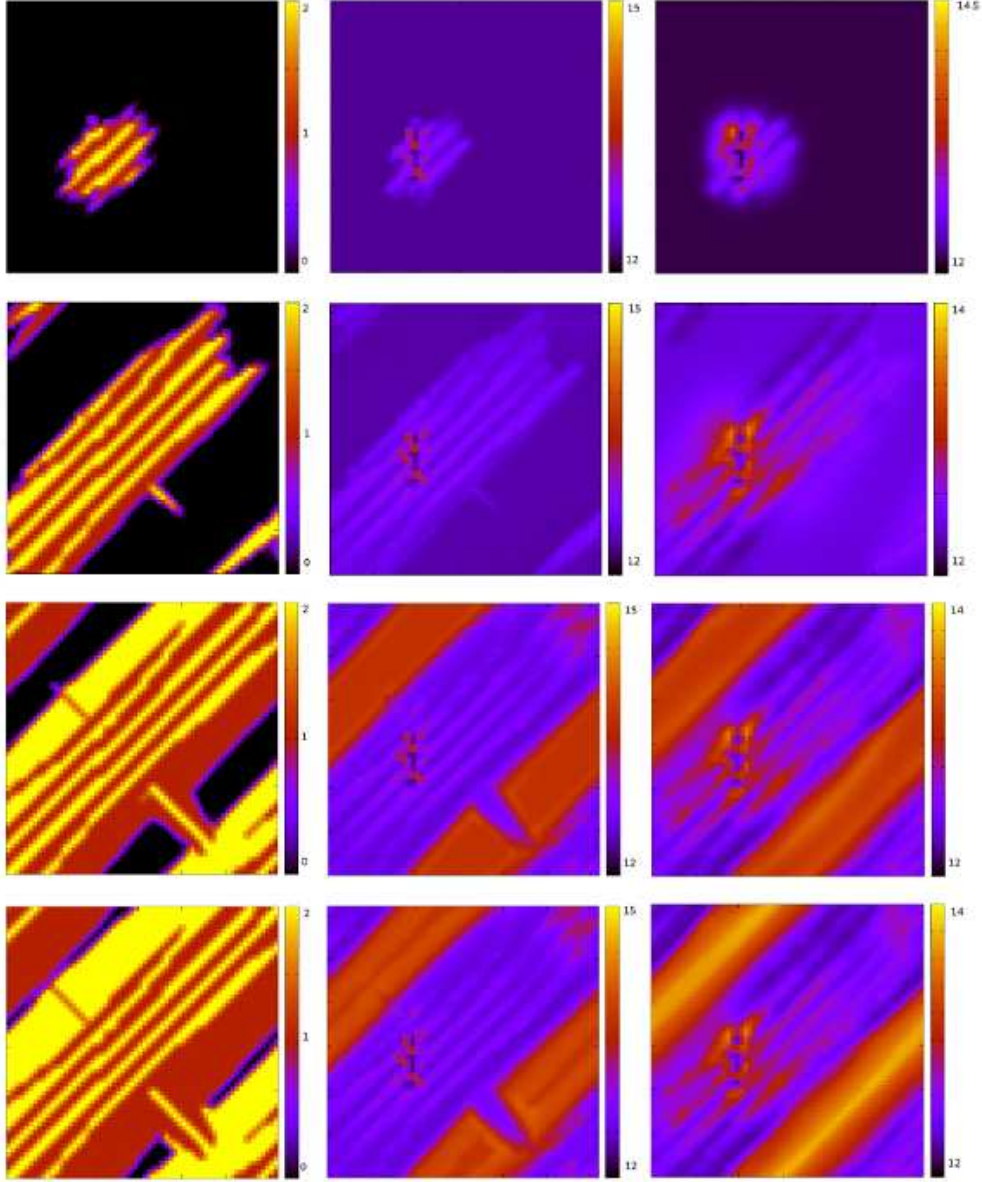


Fig. .4. Simulated microstructure and dislocation field evolution during MT in the 2D cross-sections of a 3D box of size $64\Delta x$ along $[001]$ axis with $\xi = 1.5l_0$. First column contains the microstructures at 1500, 2500, 3500 and 5000 time steps, red and yellow areas represent the 1 and 2 martensitic variants. The corresponding dislocation density field in logarithmic scale is shown in the second column without annihilation and in the third column with annihilation term.

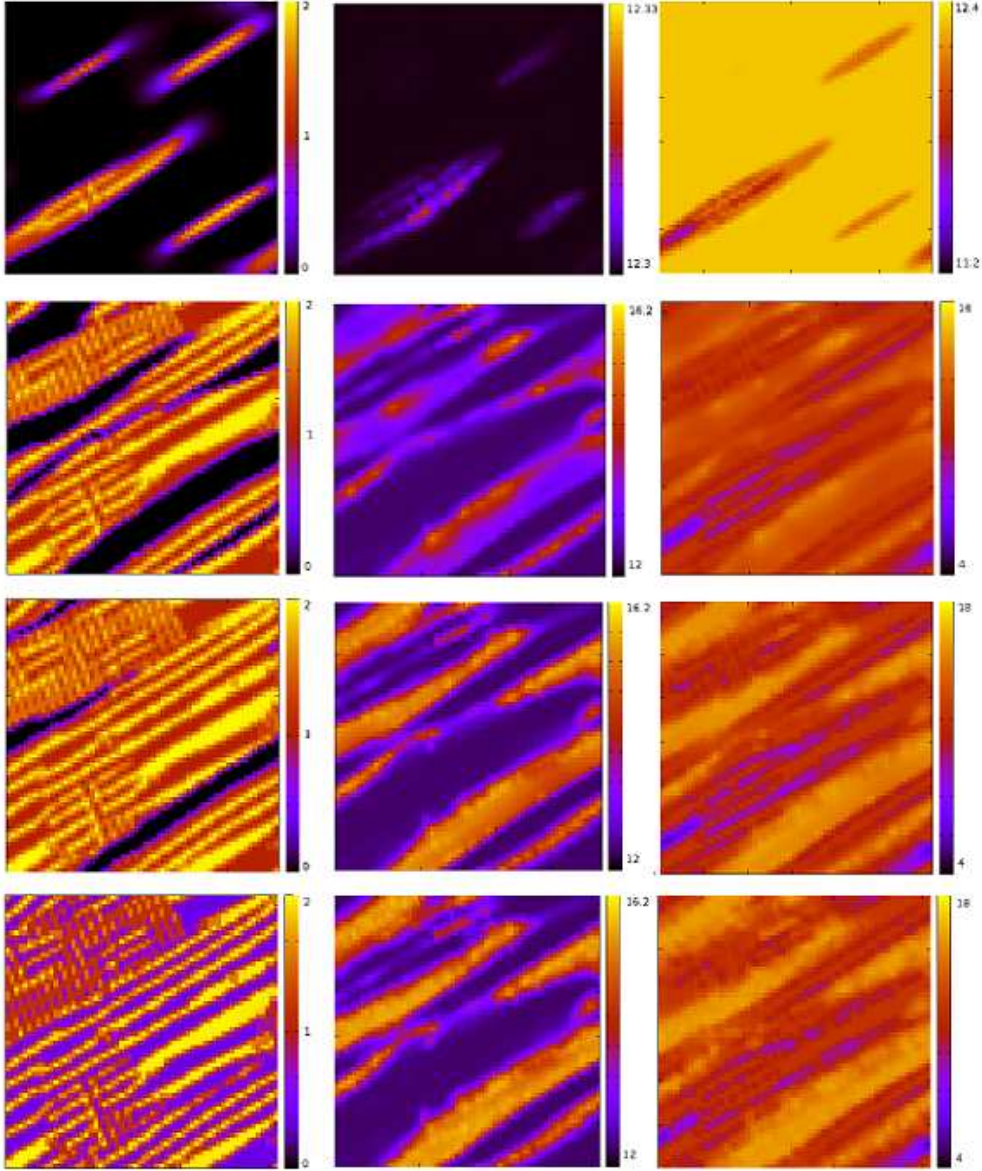


Fig. 5. Simulated microstructure and dislocation field evolution during isothermal MT in the 2D cross-sections of a 3D box of size $64 \Delta x$ along $[001]$ axis with $\xi = 0.32 l_0$ through 6 nucleus. First column represents the microstructure at 1500, 2500, 3500 and 5000 time steps, red and yellow areas represent the 1 and 2 martensitic variants. The corresponding dislocation density field is shown in the second column without annihilation and in the third column with annihilation term.

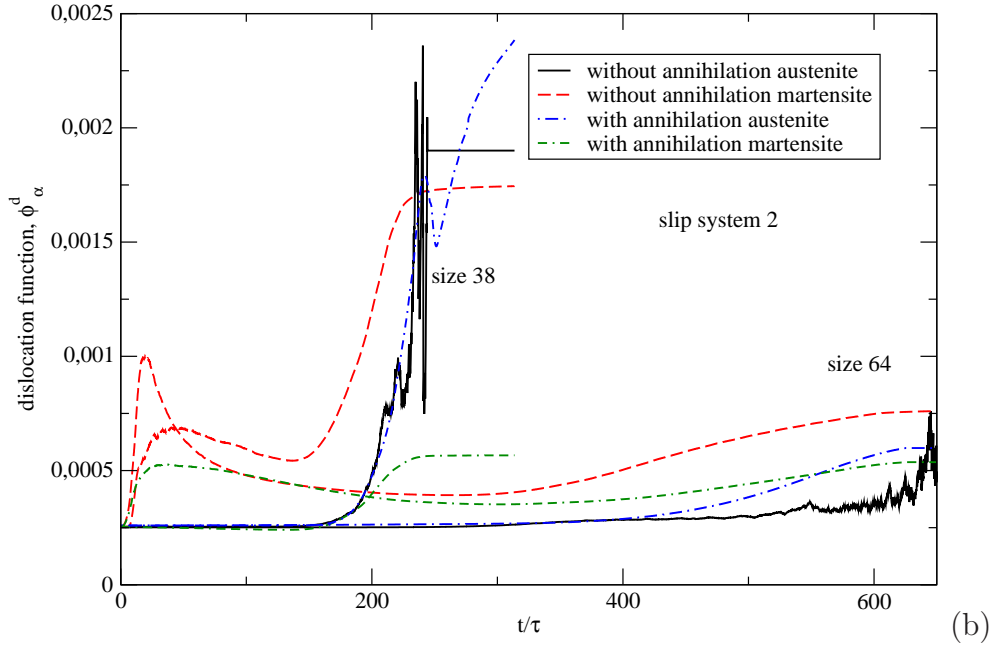
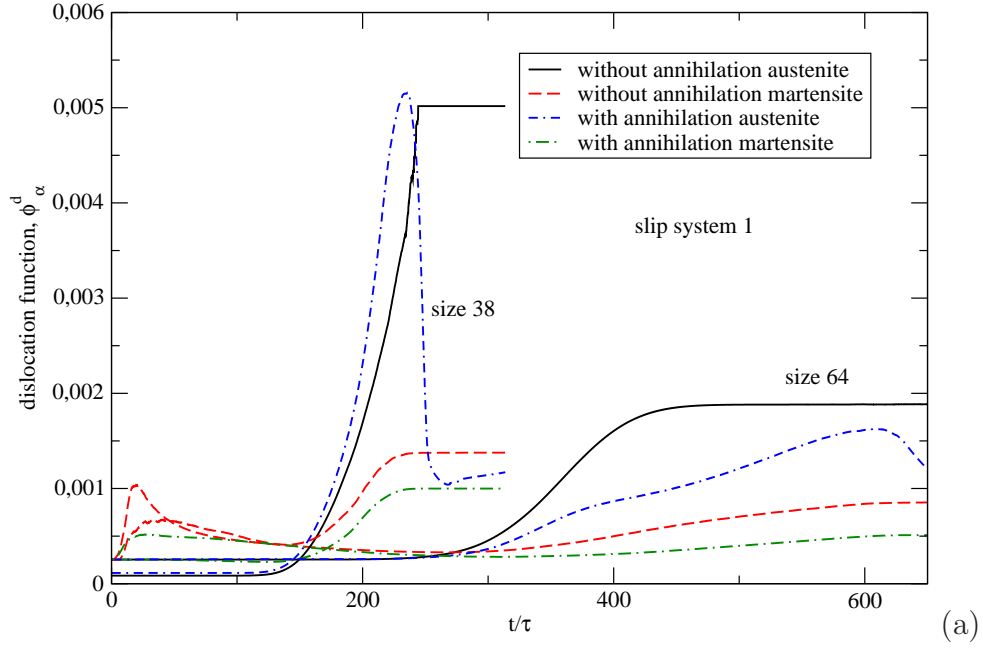


Fig. .6. Time evolution of the dislocation density function for the slip system 1 (a) and 2 (b).

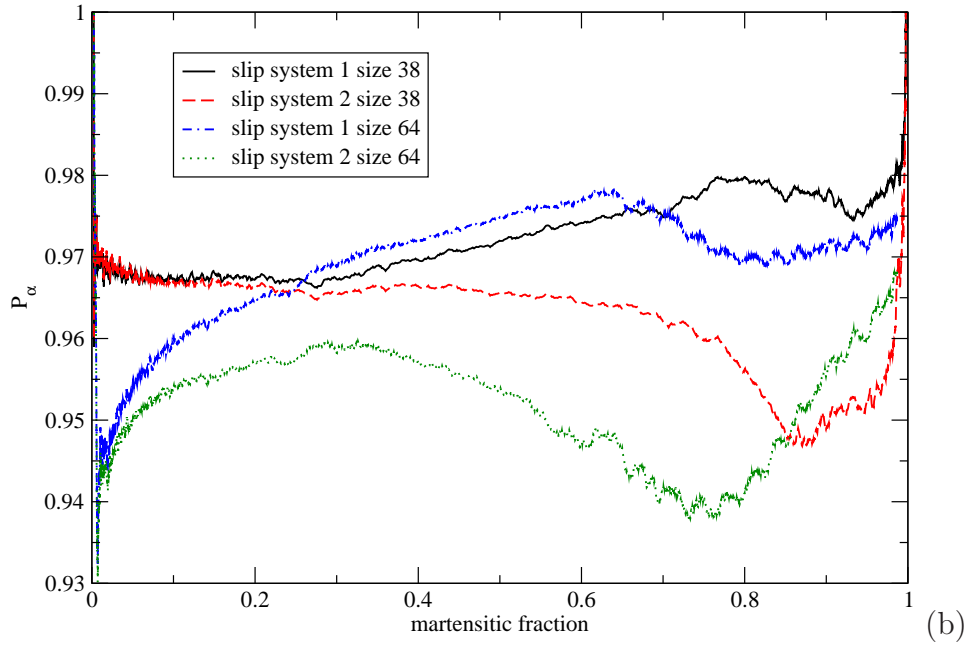
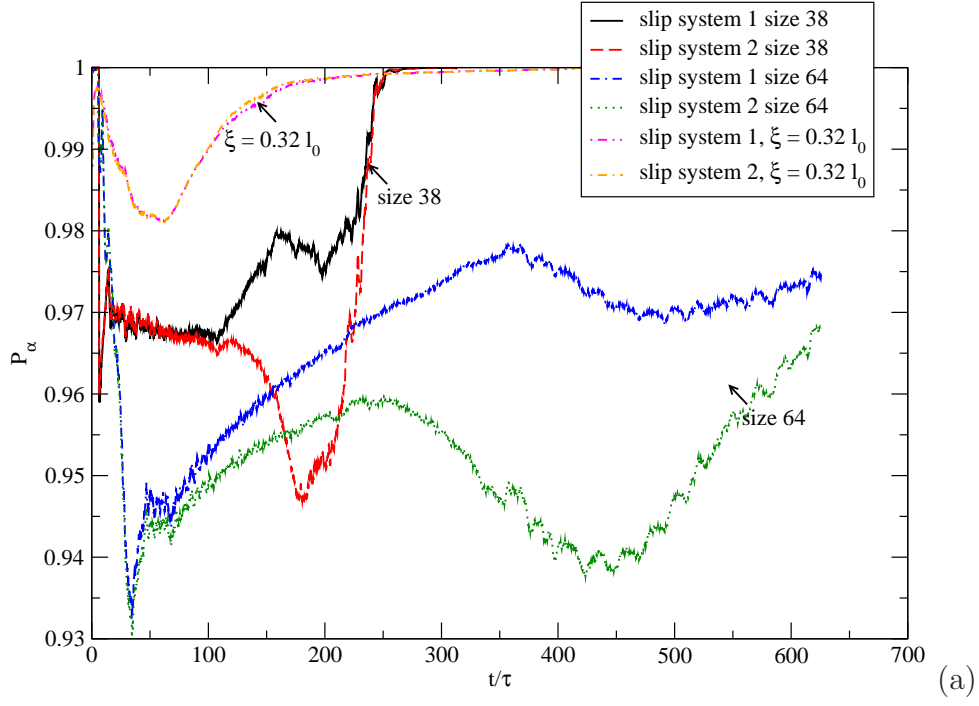


Fig. .7. Time evolution of the probability of the dilocation inheritance for slip systems 1 (a) and 2 (b).

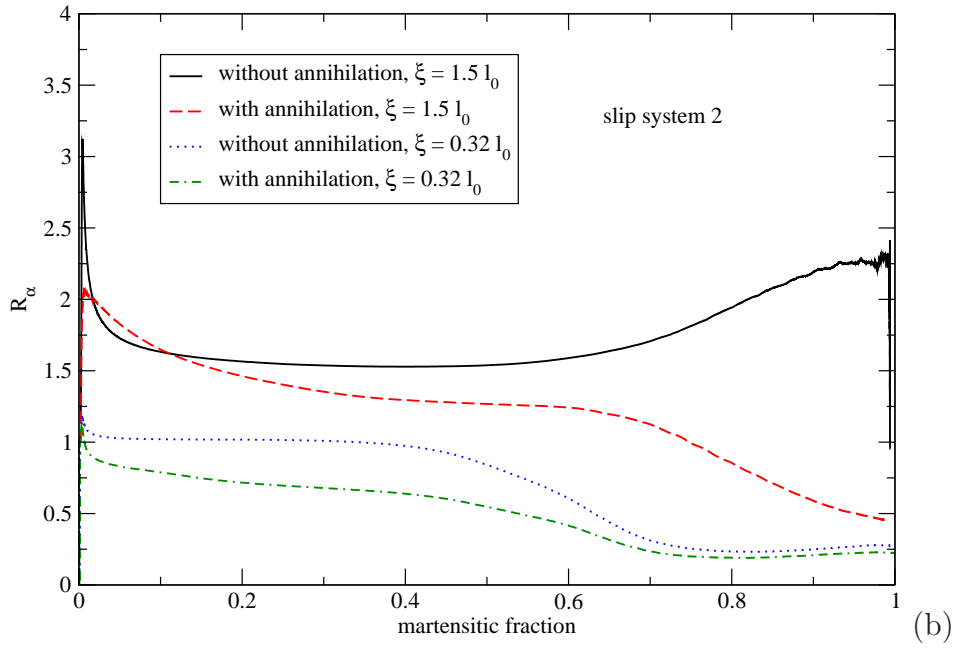
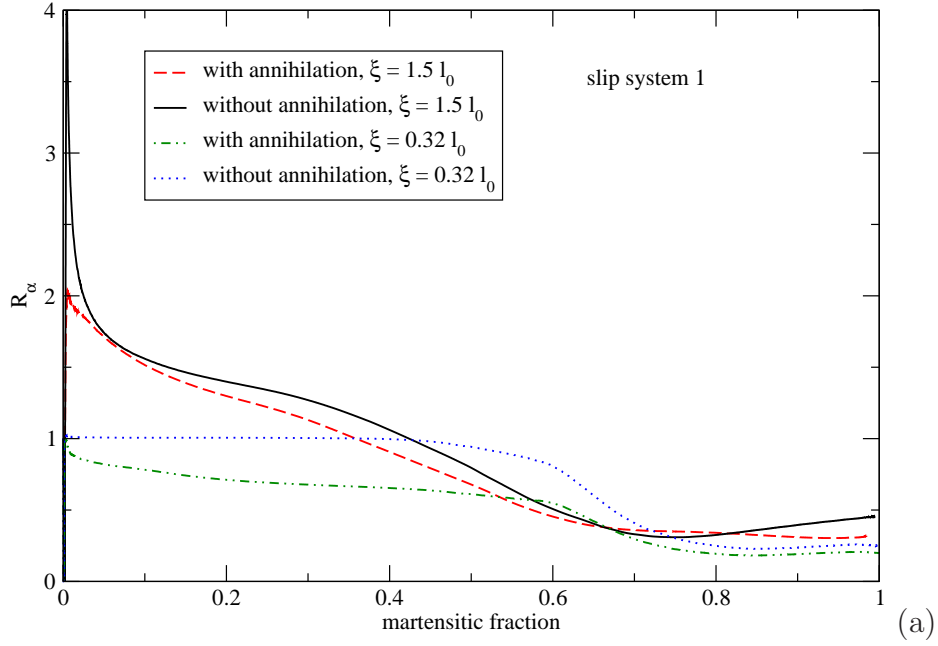


Fig. .8. Ratio between the dislocation densities in the martensite and austenite as function of the martensitic fraction with and without annihilation and diffusion for slip systems 1 (a) and 2 (b).

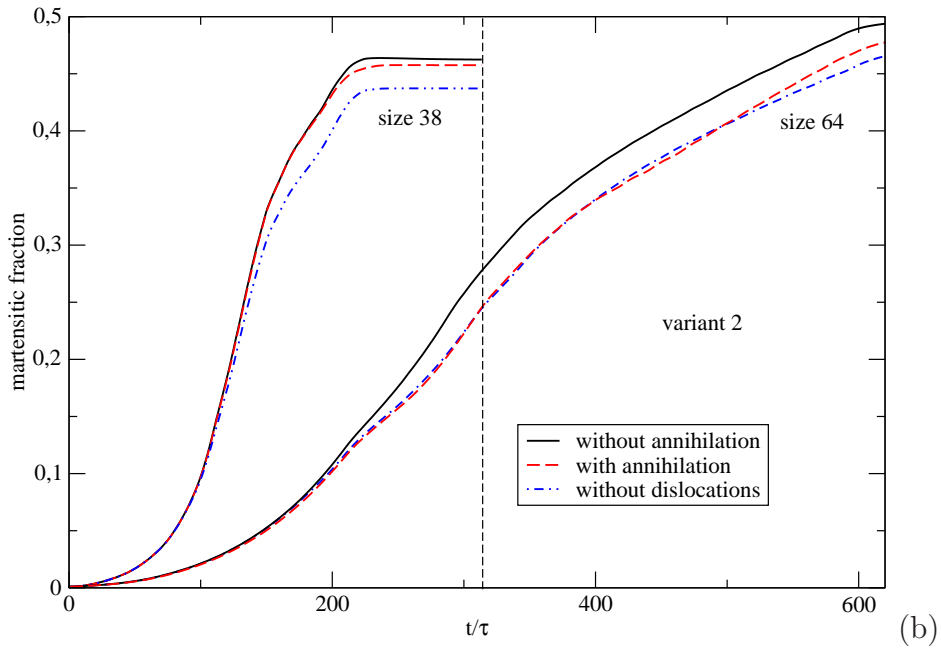
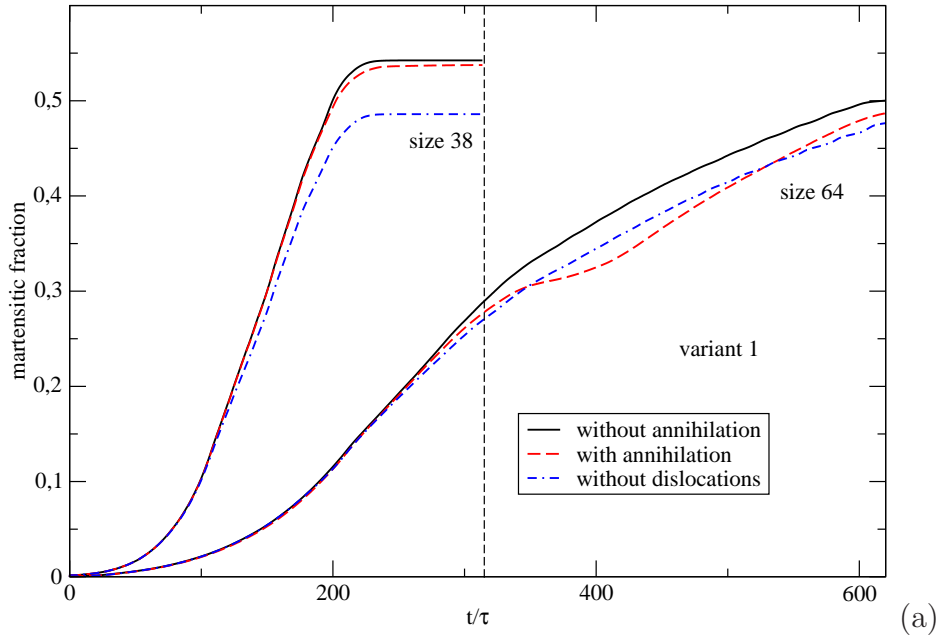


Fig. .9. Evolution of the martensitic fraction for two variants (a) and (b) with and without annihilation.